Effect of Nanoporous Structure on Enhanced Electrochemical Reaction

ARTICLE *in* THE JOURNAL OF PHYSICAL CHEMISTRY C · MAY 2010

Impact Factor: 4.77 · DOI: 10.1021/jp909382b

Effect of Nanoporous Structure on Enhanced Electrochemical Reaction

Ji-Hyung Han,[†,||] Eonji Lee,[‡,||] Sejin Park,[§,||] Rakwoo Chang,*[,‡] and Taek Dong Chung*[,†]

Department of Chemistry, Seoul National University, Seoul 151−747, Korea, Department of Chemistry, Kwangwoon University, Seoul 139−701, Korea, and Nomadien Corporation, B-206, SK Twintech Tower, Gasan-dong, Geumcheon-gu, Seoul 153-773, Korea

Received: September 30, 2009; Revised Manuscript Received: March 4, 2010

Geometric factors affecting the enhanced electrocatalysis on nanoporous Pt (L_2-ePt) were examined by electrochemical methods and computer simulations. The experimental results revealed that the electrochemical enhancement of O_2 and H_2O_2 does not come only from expansion of the active surface area (so-called roughness factor, f_R) of L_2-ePt. The presence of extra contribution was verified by the fact that significant enhancement in electrocatalytic reactions remained even after the effect of the f_R was eliminated from the electrochemical redox behavior of O_2 and H_2O_2 on L_2-ePt electrodes. Not only the voltammetric observation but also potentiometric pH responses of L_2-ePt suggested the presence of unique nanoporous effects other than the surface enlargement in regard to heterogeneous electrochemical reactions. L_2-ePt showed near Nernstian behavior, faster response time, and less hysteresis even if the real surface area was smaller than that of flat Pt. Increased residence time near the electrode surface due to extremely confined space of nanoporous structure was proposed as possible origins and examined by the Monte Carlo simulations of simple model electrodes. The theoretical approaches indicated that long residence time of reactant at electrode surface by confinement effect of the nanoporous environment well accounted for the experimental results.

1. Introduction

The porous materials have been widely addressed and utilized for a variety of applications including electrochemical sensor, fuel cell, solar cell, and battery over decades. As for nanoporous electrode materials, the evolution of the porous structures has been led by development of fabrication methods like dealloying[1] and electrodeposition in the presence of various templates such as AAO (anodized aluminum oxide),[2] self-assembly of surfactant molecules[3] or copolymers,[4] zeolite,[5] and colloidal sphere.[6]

Since electrocatalytic activity can be considerably enhanced by the nanoporous electrode materials, the electrocatalysis at nanoporous surface has been attracting much attention. The origin of the electrocatalysis at the porous electrodes has been generally ascribed to enlargement of the surface area. Indeed, the enlarged electroactive surface area is the largest reason for the catalytic power of porous electrodes in the sense that larger surface should provide reactants with more chances of interaction. However, it is questionable assumption that the enlarged surface area of porous structures is the only factor facilitating electrochemical reactions. Besides the surface area itself, the porous structure offers unique environment that is potentially favorable for electrocatalysis. For instance, the high surface-to-volume ratio allows even shorter average distance between the reactants and the inner electrode surface than that on a flat electrode so that three-dimensional (3D) interaction between inner walls and reactants in the pores could be remarkably promoted.[7,8] Furthermore, the dynamics of the reactants in the pores is confined in the space that is surrounded by the electrode surface and thereby collision events of a reactant are expected to take place more frequently.[9,10] As the pore size is reduced, it is predicted that these geometric contributions become increasingly significant.

The theoretical studies on porous structure effect have been extensively conducted with respect to the dynamics of molecules inside nanopores. Coasne et al. reported that pore connectivity affects the adsorption/condensation of gas in mesoporous micelle-templated silica (MCM-41, MCM-48, and SBA-15).[8] And, the effect of surface roughness of porous media on self- and transport diffusion in the Knudsen regime was investigated by Malek and Coppens.[10] They reported that self-diffusivity decreases with increasing surface roughness leading to increased trajectory length of a molecule and the effect of roughness on self-diffusion is less pronounced as pore diameter is wider. Sonwane and Li estimated surface transport of gases in a coarsened, densified, and bimodal porous system with unbiased random walk of tracer atom on the pore surface.[11] However, these simulation results were based on inorganic nanoporous materials such as zeolite, which do not have electrocatalytic ability but potential applications like gas storage. To achieve more powerful electrocatalysis from nanoporous electrodes, it is necessary to probe the correlation between nanoporous structure and enhanced electrocatalysis. Theoretical simulation is one of the promising approaches.

The pore effect to the electrocatalytic activity has been investigated mostly by controlling the pore sizes of mesoporous electrodes. Chai et al.[12] developed a synthetic method to fabricate ordered uniform mesoporous carbon frameworks with pore sizes in the range of 10−1000 nm and showed that the smaller pore size in the porous carbons gives the better catalytic activity for methanol oxidation. Du et al.[13] also demonstrated the relationship between O_2 reduction activity and the pore size of mesoporous carbon aerogel. These works reached a similar

* To whom correspondence should be addressed. E-mail: (R.C.) rchang@kw.ac.kr; (T.D.C.) tdchung@snu.ac.kr. Phone: (82) +2-880-4354 Fax: (82) +2-887-4354.
[†] Seoul National University.
[‡] Kwangwoon University.
[§] Nomadien Corporation.
[||] E-mail addresses: (J.-H.H.) tttre6@snu.ac.kr; (E.L.) ukjigirl@kw.ac.kr; (S.P.) yyeppi@snu.ac.kr.

10.1021/jp909382b
Published on Web 05/06/2010

conclusion that about 20 nm is the optimal pore diameter of the mesopores for electrocatalysis, resulting from the compromise between the surface area and mass transport in the porous structures. For electrochemical reactions with sluggish charge transfer kinetics, the pore size needs to be further reduced. The representative example is the microporous metals based on zeolite on which platinum,[14] ruthenium,[15] and gold[5] are loaded. The zeolite structures can play the roles of not only a cation selective membrane but also a molecular-sized cage. However, faradaic reaction hardly occurs in such minute pores[16] because the pore diameter of zeolites is less than 1 nm, which is definitely thinner than the thickness of electric double layer (EDL) in normal electrolyte solutions. Moreover, the pores less than 1 nm in diameter are too narrow for reactant molecules to be transported into deeper region. In this regard, nanoporous materials with pore diameter of 1−10 nm, which is the ultimate pore size comparable with the thickness of EDL, are expected to possess unusual potential for electrocatalysis of electrochemically sluggish reactions. This range of pore size corresponds to the smallest scale, which meets the condition that electrochemically effective electrode area is identical to the geometrically enlarged surface.[16]

The representative examples are nanoporous Pt films (H_1-ePt[3] and L_2-ePt[17]) electroplated in the surfactant templates. H_1-ePt and L_2-ePt stand for the electrodeposited platinum films in hexagonal(H_1) and reverse micelle(L_2) phases, respectively. These electrode materials have pore diameter of 1−3 nm, which is close to microporous dimension, and exhibit outstanding electrocatalytic power on various electrochemical reactions. Birkin et al. reported the electrochemical reduction of aqueous O_2 on H_1-ePt microelectrodes.[18] They found that the limiting current due to the O_2 reduction is significantly higher on H_1-ePt than on flat Pt and the onset potential of the O_2 reduction is positively shifted. Catalytic activity of the redox reactions of H_2O_2 at H_1-ePt was studied by Evans et al.[19] According to their results, H_1-ePt microelectrodes can produce highly enhanced faradaic current for both reduction and oxidation of H_2O_2, whereas flat Pt microelectrodes show low and ill-defined behavior. We also reported selective amplification of the sluggish electrochemical oxidation of glucose for enzyme-free glucose sensor and a novel solid-state pH sensor showing near-Nernstian behavior (e.g., −55 mV/pH in PBS) based on H_1-ePt[20,21] and L_2-ePt electrodes.[17] Despite the interesting approach and valuable information from the previous reports, these works on nanoporous electrode materials lack in depth understanding of the mechanisms or factors responsible for the enhanced electrocatalysis other than surface enlargement. There has been experimental evidence that suggests the presence of other factors that are not originated from the roughness factor (f_R) but from the nanostructure itself. The onset potential in the voltammetric reduction of O_2 and H_2O_2 markedly shifts on the nanoporous Pt films compared with the flat electrodes.[18,19] More evidently, the current due to glucose oxidation at a flat Pt is substantially lower than the value extrapolated from the linear dependence on f_R of nanoporous Pt electrodes (Supporting Information Figure S1).[20]

In this study, we explore the unique effect of pore structures to the enhanced electrocatalysis on nanoporous electrodes, L_2-ePt. The enhancement due to f_R is eliminated by employing the amperometric current density, which is defined as current divided by active electrode surface area (j_{real}), instead of apparently recorded current (i) or current density normalized by geometric surface area (j_{app}). Potentiometric responses to pH are also investigated in terms of response time, linearity, and hysteresis to confirm the geometric pore effect through comparison study on the electrochemical signals from flat macroelectrodes and L_2-ePt microelectrodes with similar real surface areas. The origins of the extra electrocatalytic enhancement in nanoporous structure are theoretically probed through Monte Carlo (MC) simulations of random porous and planar systems, too.

2. Experimental Methods

2.1. Reagents. All the chemicals including hydrogen hexachloroplatinate hydrate, Triton X-100, sulfuric acid, sodium chloride, hydrogen peroxide, phosphoric acid, sodium phosphate, and Pt wire were purchased from Aldrich and used without further purification. Phosphate buffer saline (PBS) was prepared by mixing 0.1 M H_3PO_4 and 0.1 M Na_3PO_4 containing 0.15 M NaCl. All electrochemical tests for O_2 and H_2O_2 were carried out in a temperature controlled cell, which has 10 mL of 0.1 M PBS at pH 7.4 and 25 °C

2.2. Instrumentation. Amperometric electrochemical experiments were performed using an electrochemical analyzer (model CH660, CH Instruments Inc.). Hg/Hg_2SO_4 (saturated K_2SO_4, CH Instruments Inc.) and Pt wire (diameter 0.5 mm) were used as reference electrode and counter electrode, respectively. Pt microelectrodes (diameter 25 μm, CH Instruments Inc.) were used as a substrate electrode for the L_2-ePt film and a flat electrode. Potentiometric pH measurements were performed using a homemade multichannel potentiometer. A combination pH electrode (ROSS 8102, Orion) was used to check pH during E_{oc} measurement. An Ag/AgCl (saturated KCl, CH Instruments Inc.) and a platinum rod electrode (diameter 0.25 mm) were used as reference and flat working electrodes, respectively. A Pt microelectrode (diameter 25 μm) was the substrate on which L_2-ePt was electrodeposited.

2.3. Electrodeposition of L_2-ePt. Hydrogen hexachloroplatinate hydrate (5 wt %), 0.3 M NaCl (45 wt %), and Triton X-100 (50 wt %) were mixed and heated to 60 °C. The mixture as made was transparent and homogeneous. The temperature of the mixture solution was maintained around 40 °C using a thermostat, and therein electrodeposition of L_2-ePt was carried out on a Pt microelectrode at −0.2 V versus Ag/AgCl. The resulting L_2-ePt electrode was placed in distilled water for 1 h to extract the Triton X-100, and the extraction procedure was repeated 3−4 times. Then the electrode was electrochemically cleaned by cycling potential between +0.68 and −0.72 V versus Hg/Hg_2SO_4 in 1 M H_2SO_4 until reproducible cyclic voltammograms were obtained.

2.4. Electrochemical Experiments. The surface areas of the Pt electrodes were determined from the hydrogen adsorption/desorption peaks of the cyclic voltammograms (scan rate, 200 mV s^{-1}) in 1 M sulfuric acid solution based on 210 μC cm^{-2} of the conversion factor.[22] Before amperometric and potentiometric experiments, electrochemical cleaning of electrodes was conducted by cycling potential between +0.68 and −0.72 V versus Hg/Hg_2SO_4 in 1 M H_2SO_4 to get rid of residual contaminants on the electrode surfaces. Linear sweep voltammetry (LSV) of H_2O_2 and O_2 were carried out in 10 mL solution of 0.1 M PBS containing 0.15 M NaCl. Linear sweep voltammograms of H_2O_2 and O_2 were obtained after purging N_2 and O_2, respectively, for 20 min. For potentiometric pH measurements, platinum oxide layer was formed on the electrode surface by applying 0.6 V versus Ag/AgCl to a Pt electrode in a PBS solution at pH 7.4 for 600 s. The resulting electrode was then stabilized in a PBS solution for a half day. The potential responses (E_{oc}) to pH were monitored in unstirred and air-saturated PBS solutions and recorded at 200 s after pH changes.

Response times at a variety of pHs were measured in stirred PBS solutions by adding 2 M H_3PO_4 containing 0.15 M NaCl. Reference electrode was an Ag/AgCl (saturated KCl).

2.5. Computer Simulation. We have performed grand canonical Monte Carlo Simulations (GCMC) to investigate the effect of surface geometry on the enhanced electrocatalysis of nanoporous electrodes. The reactant molecules were modeled as hard-spherical particles and the electrode was regarded as a hard-solid matter. Two different categories of electrode geometries were examined in this study: planar surface and random porous geometries. The planar surface geometry was modeled as a slit, where two parallel planar surfaces were separated by $L = 40$ nm, which is shown in Figure S2A in Supporting Information. For random porous geometries, chains of eight connected hard spheres with diameter of $\sigma_R = 3.0$ nm were equilibrated in a 20 nm × 20 nm × 20 nm simulation box, immobilized under the condition of the volume fraction $\phi = 0.2$, and replicated four times in the x and y directions and eight times in the z direction to form a porous material with the dimension of 80 nm × 80 nm × 160 nm. Finally, a simulation box of 80 nm × 80 nm × 200 nm was constructed, where both a porous material region (80 nm × 80 nm × 160 nm) and a bulk solution region (80 nm × 80 nm × 40 nm) coexist. The periodic boundary condition was then imposed to the resulting simulation box as shown in Supporting Information Figure S2B. In this system, the average distance between immobilized hard spheres in the porous region is around 4.1 nm. For both electrode geometries, the center of the bulk solution region was set to $z = 0$ nm, which is 20 nm away from the surface.

To probe the dependence of collision encounter on the geometry of electrode materials, the interaction between a reactant and the electrode surface was simply given by a square-well potential

$$U_{HS}(r) = \begin{cases} \infty & r < 0 \\ -\varepsilon & 0 \le r < d \\ 0 & r \ge d \end{cases}$$

where r is the shortest distance between the reactant and the surface and ε and d are the reactant-surface interaction parameters. The strength of interaction between reactants and a surface in an aqueous solution is not well-known yet. Although theoretical adsorption energy was calculated mostly in air condition, there are a few reports that addressed the interaction energy in water environment. The representative work was conducted by Janik et al.[23] They investigated adsorption property of O_2 molecules at the solvated and electrified Pt(111) interface and calculated minimum relative binding energy (0.3 eV = 29 kJ mol^{-1}), which is required for replacement of adsorbed water by O_2 molecule. The binding energy obtained in this work is significantly low compared to the results in gas phase and more appropriate for real electrochemical environment considering the aqueous system in the present study. However, they ignored the interaction between electrolyte ion and electrified surface. It is well-known that strong adsorption of anions (chloride, sulfate, iodide, etc.) interferes in adsorption of O_2 molecule and hampers the electron transfer.[24] Therefore, it is expected that real adsorption energy of O_2 molecule in electrochemical environment is much less than simulation value. Therefore, ε and d were respectively set to 0.0−20.0 kcal mol^{-1} and 0.5 nm in this study. The interaction between reactant molecules was also given by a hard-spherical potential with the diameter of 1.0 nm. Since the concentration of the reactant molecules is very low (1 mM = 0.0006 molecules nm^{-3}), the simulation results are not supposed to be sensitive to the interaction parameters.

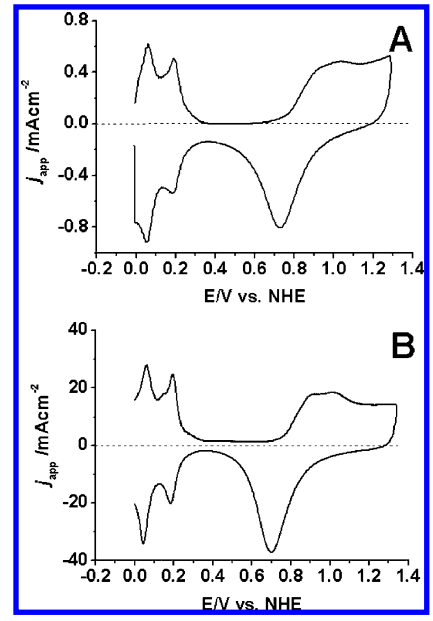

Figure 1. Cyclic voltammograms of (A) flat Pt (f_R 2.68, $A_{app} = 7.8 \times 10^{-3}$ cm^2) and (B) L_2-ePt (f_R 122, $A_{app} = 7.8 \times 10^{-3}$ cm^2) in 1 M H_2SO_4 in aerobic condition.

In the GCMC simulations, reactant molecules corresponding to 1 mM in a bulk solution are created or vanished in the region of $z = -15$ to +15 nm to keep the reactant concentration to 1 mM in the bulk solution region. Then, reactant molecules were allowed to move by random walk with the step size of 1.0 Å and the time step of 1.667 ps with the diffusion coefficient of 1.0×10^{-5} cm^2 s^{-1} in a bulk solution region. Each trial is accepted or rejected based on the Metropolis algorithm.[25] In addition to creation, removal, and translational moves, an additional motion was employed in the simulation to mimic redox reactions. A reactant molecule within a cutoff distance, r_{coll}, from the surface is removed if it stays longer than a given reaction time, τ. In this study, r_{coll} was set to 0.5 nm and τ was varied from 1 to 10^3 ns. Each system was equilibrated until the distribution of the reactant molecules reached the steady state. The equilibrated system was then used as an initial configuration for ensemble sampling. Each system was sampled every 10^3 GCMC steps (translation 40%, creation 30%, removal 30%) and the number of sampling ranged from 10^4 to 3×10^4 depending on the reaction time.

3. Results and Discussion

3.1. Surface Crystal Facets of L_2-ePt. The effect of crystallites on electrocatalysis has been a big issue in the surface electrochemistry since the degree of anion adsorption and the hindrance effect of absorbent are very sensitive functions of the crystal facets. That is why synthetic methods have been sought to find solid electrode materials with specific facets that catalyze particular reaction such as O_2 reduction.[26] In this regard, it is conceivable that the enhanced electrochemical reactions on L_2-ePt might be attributed to a specific crystalline facet. However, Figure 1 shows that both L_2-ePt and flat Pt are polycrystallines and exhibit indistinguishable electrochemical behavior. The cyclic voltammograms of L_2-ePt and flat Pt are slightly different in terms of not only the typical waves of hydrogen adsorption/desorption but also the oxide layer forma-

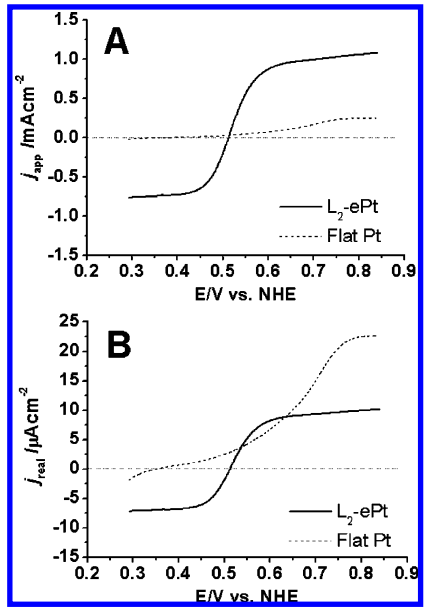

Figure 2. Linear sweep voltammograms of microflat Pt (diameter 25 μm, f_R 11) and L_2-ePt (diameter 25 μm, f_R 148) in 0.1 M PBS containing 1 mM H_2O_2 after removing O_2 by bubbling N_2 gas during 20 min. (A) j_{app} and (B) j_{real}.

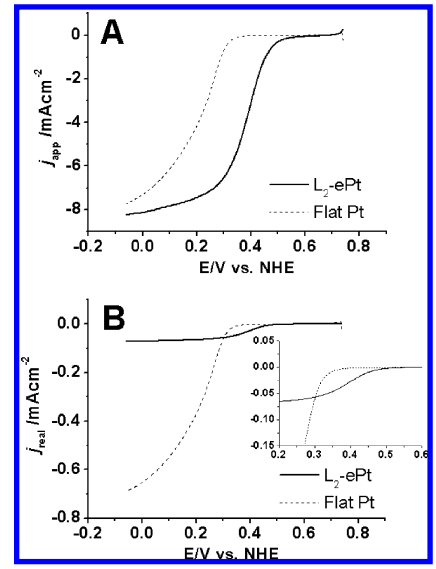

Figure 3. Linear sweep voltammograms of a flat Pt (diameter 25 μm, f_R 11) and a L_2-ePt (diameter 25 μm, f_R 148) in 0.1 M PBS after purging O_2 gas during 20 min. (A) j_{app} and (B) j_{real}. Insertion in Figure B: enlarged view of the region from 0.2 to 0.6 V.

tion and reduction. Therefore, we can rule out the crystallite effect from the candidates possibly contributing to the enhanced electrocatalysis of L_2-ePt.

3.2. Electrochemistry of H_2O_2. Electrochemical redox behavior of H_2O_2 was examined by linear sweep voltammetry in 0.1 M PBS solution (Figure 2). Figure 2A shows that both cathodic and anodic j_{app} (the current divided by apparent area) of L_2-ePt exhibit nearly reversible redox behavior of H_2O_2, consisting with the results of H_1-ePt in the previous report.[19] Especially, cathodic j_{app} of L_2-ePt was much greater than that of flat Pt. This behavior tells that nanoporous surface facilitates electrochemical oxidation and reduction of H_2O_2 than flat one. The difference in f_R (148 to 11) is responsible for the large j_{app} at the L_2-ePt, but the large shift of onset potential is not explained.

We can see the additional factor other than f_R more clearly by plotting Figure 2A again in terms of j_{real}, which is the current divided by the real surface area instead of apparent one. j_{real} in Figure 2B reflects the current density of the unit surface area including the inner walls and thereby the contribution of f_R is excluded. Both cathodic and anodic j_{real} of L_2-ePt still exhibit the redox behavior of H_2O_2, which is almost ideally reversible. The steady state currents of L_2-ePt in the potential range higher than +0.6 V and lower than +0.4 V indicate all reactants at the electrode surface are consumed and thereby the faradaic reactions are diffusion-controlled. Intriguingly, cathodic j_{real} of flat Pt is negligible while L_2-ePt produces dramatically enhanced j_{real}. The anodic j_{real} of L_2-ePt smaller than that of flat Pt suggests that only a part of the surface works as a working electrode. Under a diffusion-controlled condition, the reactants are immediately consumed at outer part of the nanoporous electrode as soon as transported from the bulk solution. As a result, the reactants in the deep region inside the nanoporous surface are depleted.

3.3. Electrochemistry of O_2. The nanopore effect is also found in O_2 reduction as shown in Figure 3. The onset potential of O_2 reduction at L_2-ePt shifts in the positive direction as shown in Figure 3A. And Figure 3B shows that cathodic j_{real} of L_2-ePt is larger than flat Pt near the onset potential of flat Pt around 0.35 V, where is kinetic-controlled region in the charge transfer. At the diffusion controlled regime at more negative potential than around 0.3 V, cathodic j_{real} of flat Pt exceeds that of L_2-ePt. Supposedly, the inner area of the electrode surface does not take part in the faradaic reaction due to the depletion of O_2 molecules, which is the same reason as that for aforementioned H_2O_2 oxidation at L_2-ePt.

3.4. Potentiometric Response to pH. The structural effect of nanoporous surface is also found in the potentiometric pH response even though the signals come from the equilibrium between the electrode surface and the solution instead of faradaic reaction. Potentiometric signals are the difference in open circuit electric potential, E_{oc}, and the E_{oc} of conducting oxides is determined by the redox equilibrium as follows.[27]

$$MO_x + 2\delta H^+ + 2\delta_e^- \overset{i_0}{\leftrightarrow} MO_{x-\delta} + \delta H_2O$$

Higher exchange current, i_0, leads to more rapid equilibration, resulting in fast response to pH and stable E_{oc}. It is obvious that larger surface area gives rise to higher i_0 and thereby faster potentiometric response. If a nanoporous electrode provides faster and more stable pH response than flat one owing to their structural feature rather than enlargement of the surface area, a L_2-ePt microelectrode should exhibit better potentiometric signals than a flat Pt macroelectrode with a comparable or larger real surface area.

Figure 4A shows E_{oc} responses of L_2-ePt and flat Pt to a pH shift from 7.4 to 2.0. Although the real area of L_2-ePt was less than a half of flat Pt, L_2-ePt shows larger pH shift and shorter pH response time ($T_{95\%}$ of ~60 s) than flat Pt ($T_{95\%}$ of ~200 s). Similar results were reproducibly observed in several tens of pH response tests. The pH sensitivities of L_2-ePt and flat Pt are presented in Figure 4B,C, respectively. L_2-ePt shows near Nernstian behavior with a slope of −51 mV per pH, whereas flat Pt gives −42 mV per pH. Moreover, L_2-ePt exhibits better linearity over a wide pH range and effectively suppresses hysteresis compared to flat Pt. These results add the evidence supporting that the structural effect of nanoporous electrodes

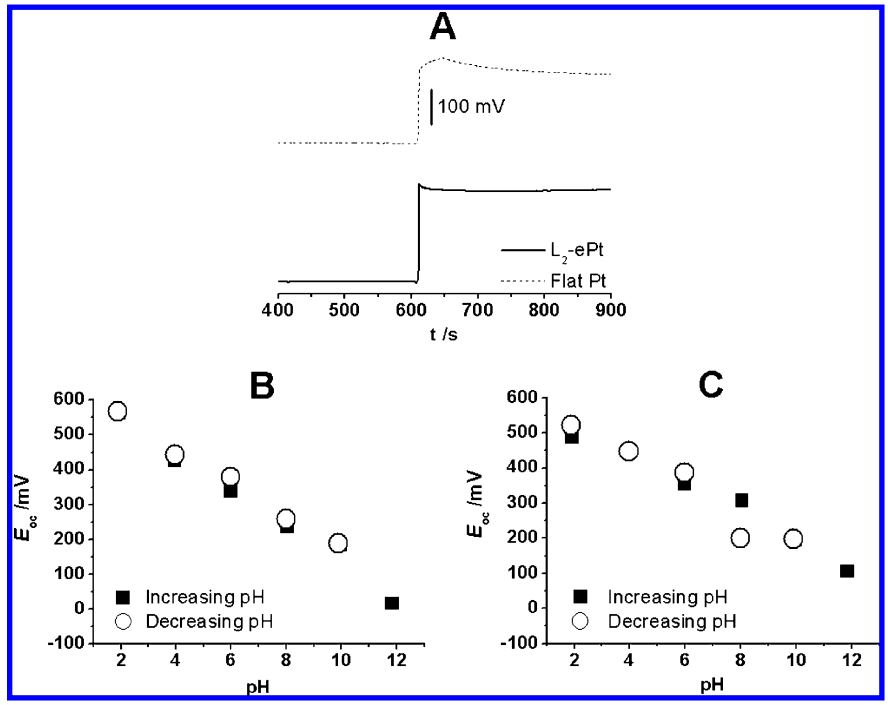

Figure 4. (A) Potentiometric responses of L_2-ePt microelectrode and flat Pt macroelectrode to a pH shift from 7.4 to 2.0. E_{oc} was recorded in an aerated and stirred PBS solution. Real area: L_2-ePt (6.0×10^{-4} cm^2), flat Pt (1.4×10^{-3} cm^2). E_{oc} versus pH curves of (B) L_2-ePt microelectrode (diameter 25 μm) and (C) flat Pt macroelectrode (diameter 0.25 mm) in unstirred and air-saturated PBS solutions, which were prepared by mixing 0.1 M H_3PO_4 and 0.1 M Na_3PO_4 containing 0.15 M NaCl. E_{oc} was recorded at 200 s after the pH was changed. pH was elevated from 2 to 12 (solid squares) and then decreased to 2 (open circles).

significantly contributes to the fast and stable responses in potentiometry as well as the enhancement in amperometry.

3.5. The Presence of Additional Factors for Electrocatalysis on Nanoporous Electrodes. As observed in H_2O_2 redox and O_2 reduction, the amperometric j_{real} implies that the enhanced electrocatalysis involves additional effect of nanoporous structure other than the surface enlargement. Such an effect appears to be more manifest in the low overpotential range rather than in the diffusion-controlled regime. As shown in Figure 2 and Figure 3, the j_{real} of L_2-ePt at an excessive overpotential in the diffusion-controlled regime reaches a plateau where the limiting j_{real} is smaller than that of flat Pt. It is can be explained by noting that only a part of the electrode surface is enough to consume the reactant molecules diffusing from the bulk solution. On the other hand, entire area of the nanoporous surface participates in the faradaic reaction at a low overpotential because the charge transfer is so slow that the reactants remain even in the deepest region of the electrode. Therefore, the j_{real} of L_2-ePt is significantly larger than that of flat Pt in the low overpotential region. For the extremely slow reaction such as H_2O_2 reduction and glucose oxidation, the j_{real} of L_2-ePt is always larger than that of flat Pt even at a high overpotential because the system hardly reaches the diffusion limited state.

Considering that the j_{real} stands for the current density and thus it is free from the f_R effect, additional factor affecting the electrocatalysis at nanoporous electrode appears prominently at kinetic-controlled regime. This situation can be understood on the basis of the series path mechanism, in which adsorption−desorption equilibrium is involved.[28] Nanoporous structure has the extremely high surface-to-volume ratio and only a limited space surrounded by the inner wall. The confined space of the nanoporous structures will provide the spatial environment that makes reactant molecules remain close to the electrode surface and prevents them from escaping to bulk solution, which is called confinement effect. As the reactant molecules trapped in a porous structure spend longer time on the surface where electrochemical reaction can occurs efficiently, the electron transfer rate increases compared to that on a flat surface. On the other hand, escape of reactant molecules from the flat surface to bulk solution is highly probable so that no sufficient residence time is provided for electrochemical reactions. As shown in Figure 5C, nanoporous structure compared to flat surface offers better environments for electrochemical reactions in terms of the interaction chances with the electrode walls. Therefore, we suggest the potential contribution of enhanced residence time of reactants near the electrode surface by confinement effect of nanostructure to the extra apparent electrocatalysis in addition to the surface enlargement effect.

The improvement of potentiometric responses of the nanoporous Pt to pH changes can be also understood on the basis of the enhanced interaction between protons in the aqueous solution and the Pt surface. It is noted that such well-defined potentiometric responses come from facilitated equilibration between aqueous protons and Pt oxide (PtOx) layer. Protons in a nanoporous channel network must have even more chances to interact with the hydroxyl groups on the PtOx layer due to the confinement effect and thus result in faster and more stable equilibration. On the other hand, the probability of interaction between protons and flat PtOx surface should be low because all directions except one are open. Overall, the equilibration between aqueous protons and PtOx layer is supposedly facilitated by the nanoporous environment so that the potentiometric response becomes more rapid and stable. As a consequence, the nanoporous structure is another reason why L_2-ePt microelectrode successfully works as a solid-state potentiometric pH sensor.

3.6. Computer Simulation. Grand Canonical Monte Carlo simulations of simplified models theoretically support the geometric effect of nanoporous structure. The details of the simulations are described in the experimental section.

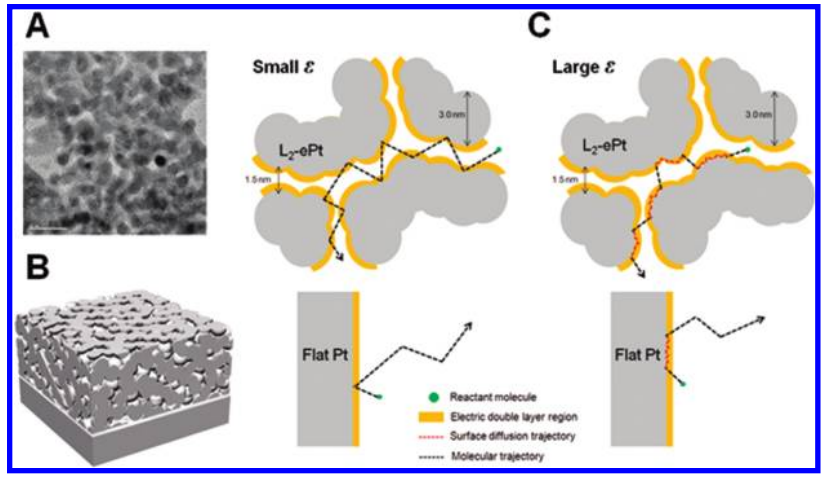

Figure 5. (A) TEM image of L_2-ePt surface. The scale bar is 10 nm. (B) Schematic view of L_2-ePt thin film. (C) Schemes for confinement effect of nanoporous Pt, L_2-ePt, at small ε and large ε between a reactant and electrode surface on the enhanced electrocatalysis.

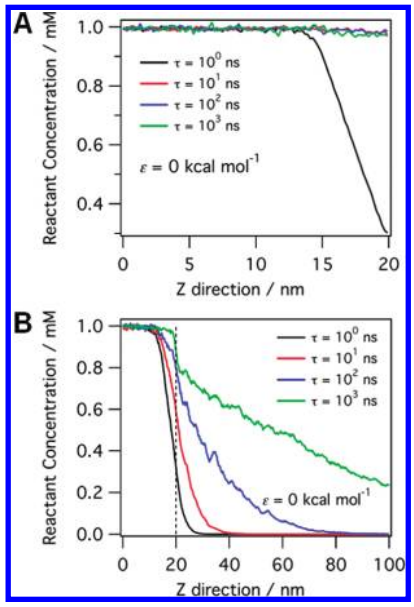

Figure 6. Concentration profiles of reaction molecules for various reaction times, τ, in both (A) planar and (B) porous geometries. The interaction strength, ε, between reactant molecules and a surface is 0.0 kcal mol^{-1} here. The dashed line in (B) represents the interfacial region between the bulk solution (left) and the porous material (right).

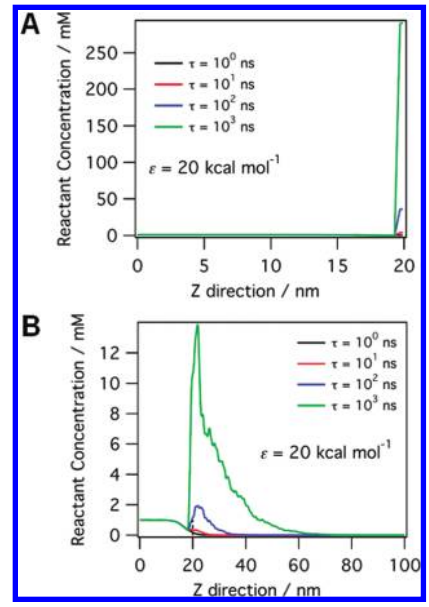

Figure 7. Concentration profiles of reaction molecules for various reaction times, τ, in both (A) planar and (B) porous geometries. The interaction strength, ε, between reactant molecules and a surface is 20.0 kcal mol^{-1} here. The dashed line in (B) represents the interfacial region between the bulk solution (left) and the porous material (right).

Figure 6 shows concentration profiles of reactant molecules along the direction normal to the electrode surface, for various reaction times in both flat and porous geometries, assuming that there is no attraction between reactants and surface ($\varepsilon = 0.0$ kcal mol^{-1}). It should be noted that molecules are continuously created or removed in the range of $z = -15$ to $+15$ nm to keep the bulk reactant concentration to 1 mM. The cutoff distance, r_{coll}, is set to 0.5 nm. When the reaction time is very short ($\tau =$ 1 ns), the reactant concentration decreases monotonically from $z = 15$ nm to $z = 20$ nm (surface) for both electrode geometries. In this regime, the redox reaction occurs much faster than the diffusion of reactant molecules, that is, the redox reaction rate is governed by diffusion (diffusion-controlled regime). As τ gets longer, the redox reaction rate on the surface is comparable to or much more sluggish than the molecular diffusion (kinetic-controlled regime) and the concentration gradient of reactant molecules near the surface becomes slower. If a reactant molecule stays within 0.5 nm from the surface for the time longer than τ, it is assumed that a reaction event occurs and the reactant is removed in the simulation system. Therefore, electrochemical reaction rarely takes place at a long τ, especially in the planar geometry. For example, for the reaction time longer than 1 ns, no reaction event was observed during the simulation of around 20 μs. In case of the porous electrode geometry, reactant molecules enter the porous region, which gives more time for the molecules to react.

The reaction rate distribution of the reaction events in the z direction is also calculated for both electrode geometries and shown in Supporting Information Figure S3. Similar to the concentration profiles in Figure 6A, the reaction events in the planar geometry occur near the cutoff distance (0.5 nm in this study) away from the surface. In case of the porous geometry, the reaction events take place mostly on the interfacial region at short τ and the distribution gets broad and its peak shifts into the porous region.

Figure 7 shows concentration profiles for both electrode geometries under a strong attractive interaction between reactants and surface ($\varepsilon = 20.0$ kcal mol^{-1}). The reaction rate distributions are also plotted in Supporting Information Figure S4. Except for the strong accumulation near the interfacial region

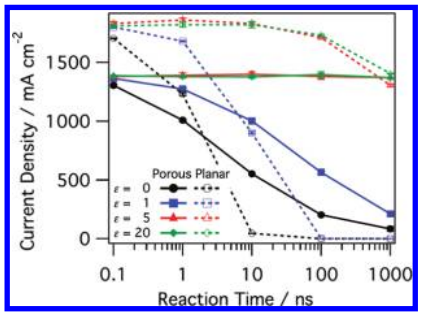

Figure 8. Current density versus reaction time in both flat and porous geometries.

and thus higher reaction signals in that region, the general feature is similar to the case of no attractive interaction between reactions and surface.

The calculated reaction events can be converted to current density, j, as a function of reaction time for $\varepsilon = 0.0$, 1.0, 5.0, and 20.0 kcal mol^{-1} in both planar and porous geometries (Figure 8). The current was calculated by assuming the redox reaction involves a single electron transfer. Without specific interaction between reactant molecules and surface ($\varepsilon = 0.0$ kcal mol^{-1}), two distinct regimes in j versus ln τ are observed: diffusion-controlled regime ($\tau \leq 1$ ns) and kinetic-controlled regime ($\tau \geq 10$ ns). In the diffusion-controlled regime, the planar electrode is expected to produce higher current density than the nanoporous electrode because most of the redox reactions occur near the interfacial region between the bulk solution and the electrode. Only outermost part of the nanoporous electrode participates in the faradaic reaction so that its current density (current divided by the entire electrode surface area) should be smaller than that of the flat electrode. On the other hand, in the kinetic-controlled regime, reaction events in the planar geometry tend to steeply drop as the reaction becomes slow (as reaction time becomes long). But the current density in the porous geometry is even less sensitive to the reaction rate. Pore confinement effect is more prominent for slower reaction. This trend of the current density as a function of reaction time (inverse of the reaction rate) is qualitatively consistent with the experimental observation. This result clearly demonstrates the confinement effect due to porous structure geometry can play a critical role in the enhancement of redox reactions, particularly for slow heterogeneous reactions.

As reactants are more strongly adsorptive to the electrode surface, that is high ε, the current density curves of planar and porous geometries cross over each other at the slower reaction rate. This indicates that the confinement effect of nanoporous structure is more effective in much slow electron transfer reaction.

Despite the new lessons suggested by the proposed model, there are some limitations in extracting more meaningful intuition from the simulation in this work. First, this model has neither atomistic details of reactant and electrode surfaces nor consideration of specific interactions unlike recent sophisticated modeling studies by Nørskov,[29] Anderson,[30] and other researchers.[31] Nonetheless, the modeling study in this work effectively supports the presence of the pure geometric effect that is distinguished from the conventional surface enlargement effect. Second, our model ignored the effects of products of the redox reaction and the reacted molecules were just removed instantaneously in the simulation. It should be considered that the accumulation of products inside porous materials may affect the reactivity of the porous surface for more accurate prediction. More detailed and elaborate theoretical approaches would offer valuable instructions to development of better catalysts.

4. Conclusions

We addressed and confirmed the effects of the unique nanoporous geometry on improved electrocatalytic activity through both experiments and computer simulations. Although the contribution of f_R was eliminated, the L_2-ePt electrode showed enhanced current density, j_{real}, in the kinetic controlled region in the redox behavior (H_2O_2 and O_2) and better potentiometric responses to pH with fast response time, low hysteresis, and near Nerntian behavior. These phenomena are ascribed to the extremely high surface-to-volume ratio and unique geometry of nanoporous structures, which remarkably augment the residence time on the electrode surface by confinement effect. Reactant molecules in a nanoporous structure have more opportunities to stay longer on the electrode surface and undergo the corresponding reaction. Although there may be other factors responsible for the signal enhancement such as defect and stress of nanoporous metals, this study clearly demonstrated that the geometric confinement makes significant contribution to the signal enhancement, especially for slow redox reactions. The results of the present study provide us with valuable lessons that the structural design and dimension of the porous catalysts are as crucial as the chemical characteristics or surface enlargement for better biosensors, fuel cells, solar cells, and many other applications.

Acknowledgment. This work was supported by the National Research Foundation of Korea (NRF) grant funded by the Korea government (MEST) (No. 2010-0001637), the Nano/Bio Science & Technology Program (M10536090001-05N3609-00110) of the Ministry of Education, Science and Technology (MEST), and the Industrial Source Technology Development Program (10033657) of the Ministry of Knowledge Economy (MKE), Republic of Korea. R.C. also acknowledges the support of Korea Research Foundation grant funded by the Korea government (MOEHRD, Basic Research Promotion Fund) (KRF-2008-331-C00129), Korea Institute of Science and Technology Information (KSC-2009-S01-0015), and a research grant of Kwangwoon University in 2009 for this work.

Supporting Information Available: The plot of glucose current of L_2-ePt and flat Pt versus roughness factor, the model system for grand canonical Monte Carlo Simulations (GCMC), and reaction rate profiles for various reaction times. This material is available free of charge via the Internet at http://pubs.acs.org.

References and Notes

(1) Jia, F.; Yu, C.; Deng, K.; Zhang, L. *J. Phys. Chem. C* **2007**, *111*, 8424.
(2) Shin, T.-Y.; Yoo, S.-H.; Park, S. *Chem. Mater.* **2008**, *20*, 5682.
(3) Attard, G. S.; Bartlett, P. N.; Coleman, N. R.; Elliott, J. M.; Owen, J. R.; Wang, J. H. *Science* **1997**, *278*, 838.
(4) Yamauchi, Y.; Sugiyama, A.; Morimoto, R.; Takai, A.; Kuroda, K. *Angew. Chem., Int. Ed.* **2008**, *47*, 5371.
(5) Ouf, A. M. A.; Elhafeez, A. M. A.; El-Shafei, A. A. *J. Solid State Electrochem.* **2008**, *12*, 601.
(6) Jiang, P.; Cizeron, J.; Bertone, J. F.; Colvin, V. L. *J. Am. Chem. Soc.* **1999**, *121*, 7957.
(7) Miyahara, M.; Kanda, H.; Yoshioka, T.; Okazaki, M. *Langmuir* **2000**, *16*, 4293.
(8) Coasne, B.; Galarneau, A.; Renzo, F. D.; Pellenq, R. J. M. *Langmuir* **2006**, *22*, 11097.
(9) White, R. J.; White, H. S. *Anal. Chem.* **2005**, *77*, 214A.
(10) Malek, K.; Coppens, M.-O. *Phys. Rev. Lett.* **2001**, *87*, 125505.
(11) Sonwane, C. G.; Li, Q. *J. Phys. Chem. B* **2005**, *109*, 5691.
(12) Chai, G. S.; Yoon, S. B.; Yu, J.-S.; Choi, J.-H.; Sung, Y.-E. *J. Phys. Chem. B* **2004**, *108*, 7074.
(13) Du, H.; Gan, L.; Li, B.; Wu, P.; Qiu, Y.; Kang, F.; Fu, R.; Zeng, Y. *J. Phys. Chem. C* **2007**, *111*, 2040.

(14) Hasegawa, Y.; Kusakabe, K.; Morooka, S. *J. Membr. Sci.* **2001**, *190*, 1.
(15) Chen, C. F.; Wang, C. M. *J. Electroanal. Chem.* **1999**, *466*, 82.
(16) Boo, H.; Park, S.; Ku, B.; Kim, Y.; Park, J. H.; Kim, H. C.; Chung, T. D. *J. Am. Chem. Soc.* **2004**, *126*, 4524.
(17) Park, S.; Lee, S. Y.; Boo, H.; Kim, H.-M.; Kim, K.-B.; Kim, H. C.; Song, Y. J.; Chung, T. D. *Chem. Mater.* **2007**, *19*, 3373.
(18) Birkin, P. R.; Elliott, J. M.; Watson, Y. E. *Chem. Commun.* **2000**, 1693.
(19) Evans, S. A. G.; Elliott, J. M.; Andrews, L. M.; Bartlett, P. N.; Doyle, P. J.; Denualt, G. *Anal. Chem.* **2002**, *74*, 1322.
(20) Park, S.; Chung, T. D.; Kim, H. C. *Anal. Chem.* **2003**, *75*, 3046.
(21) Park, S.; Boo, H.; Kim, Y.; Han, J.-H.; Kim, H. C.; Chung, T. D. *Anal. Chem.* **2005**, *77*, 7695.
(22) Trasatti, S.; Petrii, O. A. *J. Electroanal. Chem.* **1992**, *321*, 353.
(23) Yeh, K.-Y.; Wasileski, S. A.; janik, M. J. *Phys. Chem. Chem. Phys.* **2009**, *11*, 10108.
(24) Wang, J. X.; Markovic, N. M.; Adzic, R. R. *J. Phys. Chem. B* **2004**, *108*, 4127.
(25) *Computer Simulation of Liquids*; Allen, M. P., Tildesley, D. J., Eds.; Oxford University Press: New York, 1987.
(26) Wang, C.; Daimon, H.; Onodera, T.; Koda, T.; Sun, S. *Angew. Chem., Int. Ed.* **2008**, *47*, 3588.
(27) Fog, A.; Buck, R. P. *Sens. Actuators* **1984**, *5*, 137.
(28) Anastasijevic, N. A.; Vesovic, V.; Adzic, R. R. *J. Electroanal. Chem.* **1987**, *229*, 305.
(29) Hansen, H. A.; Rossmeisl, J.; Norskov, J. K. *Phys. Chem. Chem. Phys.* **2008**, *10*, 3722.
(30) Anderson, A. B.; Albu, T. V. *J. Am. Chem. Soc.* **1999**, *121*, 11855.
(31) Panchenko, A.; Koper, M. T. M.; Shubina, T. E.; Mitchell, S. J.; Roduner, E. *J. Electrochem. Soc.* **2004**, *151*, A2016.

JP909382B